ON THE CHANNEL CORRELATION STRUCTURE OF WIDEBAND SCALE-LAG RAKE FINGERS

Adam R. Margetts and Philip Schniter

Dept. ECE, The Ohio State University, 2015 Neil Ave, Columbus, OH 43210
{margetts.1, schniter.1}@osu.edu

ABSTRACT

The scale-lag Rake receiver is designed for wideband systems employing direct-sequence spread spectrum with a large bandwidth-to-center frequency ratio, such that the typical narrowband Doppler spread assumptions do not apply to mobile channels, and is capable of exploiting the diversity that results from mobility. We derive autocorrelation expressions for scale-lag Rake channel coefficients and explore the effectiveness of principal components combining (PCC) to reduce receiver complexity while maintaining performance. Such analysis applies, for example, to ultra-wideband (UWB) radio frequency channels and underwater wideband acoustic channels.

1. INTRODUCTION

Wideband systems are defined by a ratio of single-sided bandwidth to center frequency in excess of 0.20. It is important to note that the combined effects of multipath and mobility on wideband systems are quite different than those on their narrowband counterparts. For example, in narrowband systems with a dense ring of scatterers surrounding the receiver, mobility imparts a spreading of the signal in the frequency-domain that is commonly referred to as Doppler spreading [1]. In wideband communication systems employing low data rate direct sequence spread spectrum (DSSS)—the focus of this manuscript—the effects of mobility in the multipath mobile environment are not well described by frequency-domain spreading, but rather by *scale spreading*.[1] By scale spreading, we mean that several copies of the transmitted signal combine at the receiver, each with a different dilation of the time support of the original signal. In addition, each copy may be temporally delayed by a different amount.

In this paper, we investigate the correlation structure for the wideband channel, specifically for the fingers of the wideband scale-lag Rake receiver [2] [3]. While the channel correlation structure for the time-varying narrowband case has been well studied (e.g., ring-of-scatters model [1]), relatively little work has been done in classifying mobility in wideband channels. We show that the Rake fingers are approximately stationary and that channel coherence is inversely proportional to the temporal-scale spreading induced by relative velocity between the transmitter, receiver, and scatterers. The *normalized scale spread* captures, in a single parameter, the rate of scale-lag Rake finger fluctuation, just as the normalized Doppler spread captures the rate of variations in narrowband channels. We also investigate incorporating principal components combining (PCC) [4] into the scale-lag Rake receiver to reduce receiver complexity.

This work was supported in part by The Ohio Space Grant Consortium.

[1]Note that scale-spreading is actually a general concept that applies to both narrowband and wideband systems. For example, changing the time scale of a sinusoidal signal is equivalent to shifting the signal in frequency.

2. SYSTEM MODEL

2.1. Transmit Signal

The wideband DSSS signature waveform is

$$x(t) = \frac{1}{\sqrt{N_p}} \sum_{i=0}^{N_p-1} c_i p(t - iT_o), \tag{1}$$

where $\{c_i\}$ is the length-N_p PN chip sequence, $p(t)$ is the unit-energy chip waveform, and T_o is the chip duration. The symbol duration is $T_s = N_p T_o$ seconds and the system bandwidth is defined to be $W = 1/T_o$. A PN sequence $\{c_i\}$ with chips chosen from a ternary alphabet $\{-c, 0, c\}$ may be used to model time-hopping [5] or episodic signaling [6] without affecting the analysis. The chip amplitude c is chosen such that $\mathrm{E}[c_i^2] = 1$. In this paper, we consider only baseband signaling; thus, all signals and parameters are real valued.

We linearly modulate the DSSS waveform $x(t)$ with a sequence of N_b bits $\{b_j\}$ to obtain the transmitted signal $s(t)$.

$$s(t) = \sum_{j=0}^{N_b-1} b_j x(t - jT_s). \tag{2}$$

2.2. Wideband Channel

Analogous to the spreading function in narrowband channels, the wideband channel output can be modelled by the linear transformation [2] defined by:

$$r(t) \;=\; \iint \mathcal{L}\,(a,\tau)\frac{1}{\sqrt{a}}\; s\!\left(\frac{t-\tau}{a}\right) da\, d\tau + w(t), \tag{3}$$

where $s(t)$ is the input signal, $w(t)$ is additive white Gaussian noise with two-sided power spectral density of $N_o/2$, and $\mathcal{L}\,(a,\tau)$ is the *wideband channel kernel*. Note that the wideband channel transformation is *not* shift-invariant; hence, sinusoids are *not* eigenfunctions. The wideband channel kernel $\mathcal{L}\,(a,\tau)$ quantifies the scale-lag spreading produced by the channel—the variable a corresponds to the dilation introduced by the channel, and the variable τ corresponds to the propagation delay.

2.3. Definitions

In practice, the wideband channel kernel $\mathcal{L}(a,\tau)$ has finite support: $\{(a,\tau) : a_{\min} < a < a_{\max},\ 0 < \tau < \tau_{\max}\}$, where $a_{\min}$ and $a_{\max}$ are the minimum and maximum dilation, respectively, and $\tau_{\max}$ is the delay spread. By convention, the time delay of the shortest path is zero. In this paper, we assume that the signal duration T_s is much larger than the delay spread, i.e., $T_s \gg \tau_{\max}$. This is a reasonable assumption for systems with large processing gain.

If we consider a system composed of a mobile receiver, fixed reflectors, and a fixed transmitter, the minimum dilation and maximum dilation are $a_{\min} = 1 - v_{\max}/c$ and $a_{\max} = 1 + v_{\max}/c$, respectively, where $v_{\max}$ is the maximum mobile velocity. However, we note that the wideband kernel can be used to model any dynamic geometry between the transmitter, scatters, and receiver, e.g., a turbulent underwater environment with scatterers moving at different speeds.

An important system parameter is the wideband *scale spread*: $\gamma_{\max} := \frac{a_{\max}-a_{\min}}{2} = v_{\max}/c = a_{\max} - 1$, which defines the maximum deviation from unit temporal dilation applied by the wideband channel kernel.

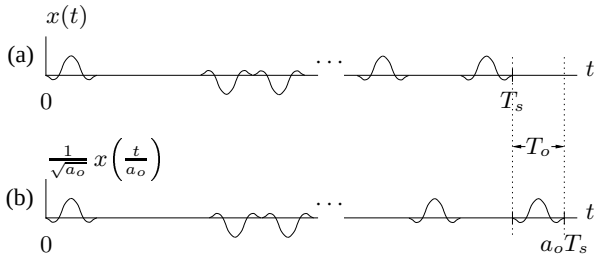

Fig. 1. (a) Transmitted wideband signal. (b) Signal dilated by a_o.

The scale-lag resolution properties of a wideband DSSS signal $x(t)$ are related to the total signal bandwidth W and symbol duration T_s. An often used rule-of-thumb is that the minimum resolvable lag of a linear Rake receiver is $T_o = 1/W$ [1]. A similar rule-of-thumb can be suggested for the *minimum resolvable dilation*, which will be defined next.

Consider the inner product of $x(t)$ with $x(t)$ dilated by a:

$$\left\langle x(t), \frac{1}{\sqrt{a}}\, x\left(\frac{t}{a}\right)\right\rangle. \tag{4}$$

Let $a = a_o$ result in a dilation by one chip period, (illustrated by Fig. 1) or in other words, let a_o satisfy the relation

$$a_o T_s - T_s \;=\; T_o \;\Leftrightarrow\; a_o = 1 + 1/N_p. \tag{5}$$

The expected value of the inner product (4) evaluated at $a = a_o$ vanishes if and only if the pulse-shape has zero DC component [3]. Hence, we define a_o as the *minimum resolvable dilation*. Equivalently, $\gamma_o := a_o - 1$ is the *scale resolution* of the wideband DSSS signal $x(t)$. We have $\gamma_o = T_o/T_s = 1/T_s W = 1/N_p$, i.e., the scale resolution is the inverse of the time-bandwidth product. Together, the scale-lag resolution properties of the wideband DSSS signal imply that $\langle x_{m,n}(t), x_{\bar{m},n'}(t)\rangle \approx \bar{\gamma}_{m-\bar{m}}\bar{\gamma}_{n-n'}$, where $x_{m,n}(t) := \frac{1}{\sqrt{a_o^m}} x\left(\frac{t-nT_o a_o^m}{a_o^m}\right)$, and $\bar{\gamma}_m$ is the Kroneker delta function.

A useful quantity is the *normalized scale spread*: $\frac{\gamma_{\max}}{\gamma_o}$ which can be written in terms of the velocity, speed of signal propagation, and the time-bandwidth product: $\frac{\gamma_{\max}}{\gamma_o} = \frac{v_{\max}}{c} T_s W$. Note the similarity to the narrowband normalized Doppler-frequency spread [1]: $f_d T_s = \frac{v_{\max}}{c} T_s f_c$, where f_c is the carrier frequency.

2.4. Scale-Lag Rake Receiver

To demodulate the i^{th} bit, the scale-lag Rake receiver projects the received signal $r(t)$ onto basis $\{x_{m,n}^{(i)}(t)\}$:

$$r_{m,n}^{(i)} \;=\; \langle x_{m,n}^{(i)}(t), r(t)\rangle, \tag{6}$$

$$\;=\; \langle x_{m,n}^{(i)}(t), \mathcal{L}\{s(t)\}\rangle + w_{m,n}^{(i)} \tag{7}$$

where $w_{m,n}^{(i)} = \langle x_{m,n}^{(i)}(t), w(t)\rangle$ are the noise coefficients. The values of m and n range over $-M \le m \le M$ and $0 \le n \le N$, where M and N are chosen so that a significant portion of the energy is retained after projection. The basis functions for the scale-lag Rake receiver are shift-dilates of the transmitted signal in order to match the scale-lag spreading of the channel. Note that the basis is time-shifted by iT_s to despread the i^{th} bit.

From the input-output relationship of the wideband kernel (3), we can write the projection coefficients $\{r_{m,n}^{(i)}\}$ as

$$r_{m,n}^{(i)} \;=\; \sum_{j=0}^{N_b} b_j \iint \mathcal{L}(a,\tau)$$

$$\underbrace{\int x_{m,n}^{(i)}(t)\tfrac{1}{\sqrt{a}} x\left(\tfrac{t-\tau-ajT_s}{a}\right) dt\, da d\tau}_{\approx 0,\ \text{for } i\neq j,\ \text{since } T_s \gg \tau_{\max}} + w_{m,n}^{(i)}, \tag{8}$$

$$\approx\; b_i \iint \mathcal{L}(a,\tau)$$

$$\int x_{m,n}^{(i)}(t)\tfrac{1}{\sqrt{a}} x\left(\tfrac{t-\tau-aiT_s}{a}\right) dt da d\tau + w_{m,n}^{(i)}, \tag{9}$$

$$\;=\; b_i \underbrace{\iint \mathcal{L}(a,\tau)\chi\left(\tfrac{a_o^m}{a}, \tfrac{nT_o a_o^m - \tau - i(a-1)T_s}{a}\right) da d\tau}_{h_{m,n}^{(i)}}$$

$$+ w_{m,n}^{(i)}, \tag{10}$$

$$\;=\; b_i h_{m,n}^{(i)} + w_{m,n}^{(i)} \tag{11}$$

where $\chi(a,\tau) := \int x(t)\frac{1}{\sqrt{a}} x\left(\frac{t-\tau}{a}\right) dt$ is the ambiguity function of the waveform $x(t)$ (similar to [7]).

To consolidate the notation, we stack the projection coefficients $\{r_{m,n}^{(i)}\}$ for the i^{th} bit into a $(2M+1)(N+1)\times 1$ dimensional vector $\boldsymbol{r}_i$, and similarly define the channel vector $\boldsymbol{h}_i$ and noise vector $\boldsymbol{w}_i$.

The scale-lag Rake generates the decision statistic $\hat{b}_i$ for the i^{th} bit by linearly combining the projection coefficients

$$\hat{b}_i \;=\; \boldsymbol{f}_i^T \boldsymbol{r}_i, \tag{12}$$

$$\boldsymbol{r}_i \;=\; b_i \boldsymbol{h}_i + \boldsymbol{w}_i. \tag{13}$$

The choice of combining vector $\boldsymbol{f}_i$ is discussed in Sec. 4.

3. CHANNEL AUTOCORRELATION

In this section, we investigate the channel autocorrelation $\boldsymbol{R}_h(i, i+j) := \mathrm{E}[\boldsymbol{h}_i \boldsymbol{h}_{i+j}^T]$. Assuming the wideband channel kernel is uncorrelated across scale and lag[2], i.e.,

[2]This simplifying assumption is analogous to the uncorrelated doppler-lag spreading assumption made in narrowband systems [8].

$\mathrm{E}[\mathcal{L}(a,\tau)\mathcal{L}(a',\tau')] = \Psi(a,\tau)\delta(a-a')\delta(\tau-\tau')$, where $\Psi(a,\tau)$ is the *wideband scattering function*, we obtain the elements of the expected outer product,

$$\mathrm{E}[h^{(i)}_{m,n}h^{(i+j)}_{m',n'}] = \int_0^{\tau_{\max}}\int_{1-\gamma_{\max}}^{1+\gamma_{\max}} \Psi(a,\tau)\,\mathrm{E}\Big[\chi\Big(\tfrac{a_o^m}{a}, \tfrac{nT_o a_o^m - \tau - i(a-1)T_s}{a}\Big)\chi\Big(\tfrac{a_o^{m'}}{a}, \tfrac{n'T_o a_o^{m'} - \tau - (i+j)(a-1)T_s}{a}\Big)\Big] da d\tau. \tag{14}$$

After we make the change of variables $\bar{\gamma} := (a-1)/\gamma_o$ and $\bar{\tau} := \tau/T_o$, the analysis in Appendix A allows us to approximate (14) with

$$\mathrm{E}[h^{(i)}_{m,n}h^{(i+j)}_{m',n'}] \approx \gamma_o T_o \int_0^{\frac{\tau_{\max}}{T_o}}\int_{-\frac{\gamma_{\max}}{\gamma_o}}^{\frac{\gamma_{\max}}{\gamma_o}} \Psi(1-\gamma_o\bar{\gamma},\bar{\tau}T_o) \bar{\chi}(m-\bar{\gamma}, n-\bar{\tau}-i\bar{\gamma})\bar{\chi}(m'-\bar{\gamma}, n'-\bar{\tau}-(i+j)\bar{\gamma}) d\bar{\gamma}d\bar{\tau}, \tag{15}$$

where we define the function $\bar{\chi}(\bar{\gamma},\bar{\tau})$ as

$$\bar{\chi}(\bar{\gamma},\bar{\tau}) := \mathrm{E}[c_i^2]\int_0^1 \chi_p(1,(\bar{\tau}+x\bar{\gamma})T_o)dx, \tag{16}$$

with $\chi_p(a,\tau) := \int p(t)\frac{1}{\sqrt{a}}p\left(\frac{t-\tau}{a}\right)dt$ as the pulse ambiguity function. The variable $\bar{\gamma}$ is the scale deviation normalized to the minimum resolvable scale deviation, and $\bar{\tau}$ is delay normalized to the minimum delay resolution. The function $\bar{\chi}(\bar{\gamma},\bar{\tau})$ approximates the expected ambiguity function: $\mathrm{E}[\chi(a,\tau)] \approx \bar{\chi}\left(\frac{a-1}{\gamma_o}, \frac{\tau}{T_o}\right)$. Note that the correlation approximation (15) depends only on the normalized scale spread $\frac{\gamma_{\max}}{\gamma_o}$ and the normalized delay spread $\frac{\tau_{\max}}{T_o}$.

For the unit-energy second-derivative Gaussian pulse[3],

$$p(t) = \frac{\sqrt{f_o}\sqrt[4]{32\pi}}{\sqrt{3}}\left[1-2(\pi f_o(t-T_o/2))^2\right] \exp\left(-(\pi f_o(t-T_o/2))^2\right), \tag{17}$$

it is shown in Appendix B that for large N_p and with $f_o := 2/T_o$,

$$\bar{\chi}(\bar{\gamma},\bar{\tau}) = \frac{1}{12}\sum_{k=0}^{4} v_k \int_0^1 x^k e^{-2\pi^2(\bar{\gamma}x+\bar{\tau})^2}dx, \tag{18}$$

$$\tag{19}$$

where $v_0 = 12-96\pi^2\bar{\tau}^2+64\pi^4\bar{\tau}^4$, $v_1 = 256\pi^4\bar{\tau}^3\bar{\gamma}-192\pi^2\bar{\tau}\bar{\gamma}$, $v_2 = 24\left(16\pi^4\bar{\tau}^2\bar{\gamma}^2-4\pi^2\bar{\gamma}^2\right)$, $v_3 = 256\pi^4\bar{\tau}\bar{\gamma}^3$, $v_4 = 64\pi^4\bar{\gamma}^4$.

To gain insight into the time-variation of the channel, we numerically evaluate the autocorrelation sequence $\mathrm{E}[h^{(0)}_{m,n}h^{(j)}_{m',n'}]$ for $m = m' = 0$, and $n = n' = 0$ and indicate the results for different values of normalized scale spread $\frac{\gamma_{\max}}{\gamma_o}$ as solid lines in Fig. 2. We assume a ring-of-scatterers model such that the scattering function $\Psi(a,\tau)$ is flat across lag τ and has a "bathtub" shape in scale a [9]. The dashed lines in Fig. 2 correspond to damped zeroth-order Bessel functions of the first kind $J_0\left(4\pi\frac{\gamma_{\max}}{\gamma_o}j\right)e^{-\frac{\gamma_{\max}}{\gamma_o}j}$, which closely approximate the autocorrelation sequence of a wideband channel with normalized scale spread of $\frac{\gamma_{\max}}{\gamma_o}$. The first zero crossing of a Bessel function $J_0(x)$ occurs at approximately $x = 3\pi/4$; it follows that the coherence time of the wideband channel is approximately $\frac{3}{16}\frac{1}{\frac{\gamma_{\max}}{\gamma_o}}T_s$ seconds. Note that the channel coherence

[3]We wish to point out that other zero-DC component signals may be used, such as the modified duobinary pulse [1].

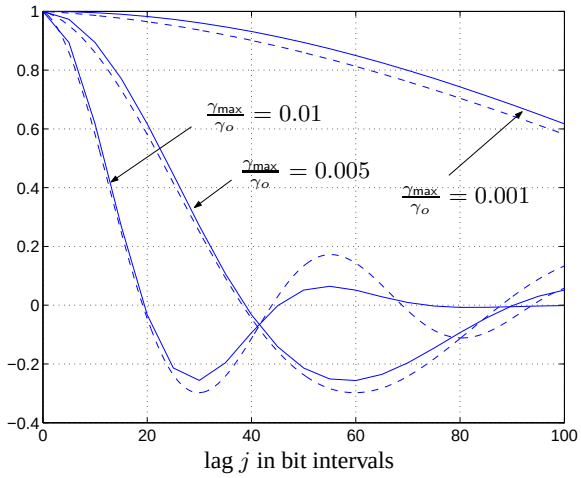

Fig. 2. (Solid lines) Channel coefficient autocorrelation sequence $\mathrm{E}[h^{(0)}_{m,n}h^{(j)}_{m',n'}]$ for $m = m' = 0$, and $n = n' = 0$. (Dashed lines) Damped Bessel function approximation: $J_0\left(4\pi\frac{\gamma_{\max}}{\gamma_o}j\right)e^{-\frac{\gamma_{\max}}{\gamma_o}j}$. The normalized delay spread is $\frac{\tau_{\max}}{T_o} = 1$.

is inversely proportional to the normalized scale spread $\frac{\gamma_{\max}}{\gamma_o} = \frac{v_{\max}}{c}T_sW$; as velocity increases, scale spreading causes greater channel variation. This is reminiscent of the role the normalized Doppler spread plays for narrowband systems.

For reference, a normalized scale spread of 0.001 would be found in an RF system with mobile velocity of 10 km/hr, data rate of 10 kbps, and bandwidth of 1 GHz, or in an RF system with velocity of 100 km/hr, data rate of 1 Mbps, and bandwidth of 10 GHz. Larger scale spreading results from increasing velocity or bandwidth and/or decreasing data rate.

3.1. Autoregressive Model for Scale-Lag Channel Coefficients

The correlation expression (15) reveals that the channel coefficients are approximately wide-sense stationary. Thus, we define the stationary correlation $\boldsymbol{R}_h(j) := \boldsymbol{R}_h(0,j)$ for generating time series realizations of the channel.

We have observed that $\boldsymbol{R}_h(j)$ can be approximately diagonalized by a common set of eigenvectors: $\boldsymbol{R}_h(j) \approx \boldsymbol{U}\boldsymbol{\Lambda}(j)\boldsymbol{U}^T$. Suppose that none of the correlation matrices in $\{\boldsymbol{R}_h(j)\}_{j=0}^{\infty}$ has more than $K_{\max}$ non-zero eigenvalues: $\{\lambda_k(j)\}_{k=1}^{K_{\max}}$. If we assume that the channel coefficients are zero-mean jointly-Gaussian processes, then channel coefficient realizations can be generated by filtering a set of $K_{\max}$ uncorrelated white noise processes. The k^{th} noise process is filtered by an autoregressive (AR) model that is fit to the k^{th} eigenvalue sequence $\{\lambda_k(j)\}_{j=0}^{\infty}$. For example, let $\{a_k(l)\}_{l=1}^{N_k}$ be the AR-N_k model parameters computed from the Yule-Walker equation. Define $z_k(i) = q_k(i) - \sum_{l=1}^{N_k} a_k(l)z_k(i-l)$, where $q_k(i)$ is white gaussian noise of suitable variance. Now define the vector $\boldsymbol{z}_i := [z_1(i), z_2(i), \ldots, z_{K_{\max}}(i)]^T$ such that the channel realization is

$$\boldsymbol{h}_i = \boldsymbol{U}_{K_{\max}}\boldsymbol{z}_i, \tag{20}$$

where $\boldsymbol{U}_{K_{\max}}$ collects the $K_{\max}$ principal eigenvectors from $\boldsymbol{U}$.

4. PRINCIPAL COMPONENTS COMBINING

In [3], we showed that the channel correlation matrix $\boldsymbol{R}_h(0)$ produces a relatively small number of non-negligible eigenvalues compared to the number of scale-lag channel coefficients. For example, Fig. 3 shows the eigenvalue spread of the system in Fig. 2. From (20), the channel dynamics are focused in a low-dimensional subspace spanned by the principal eigenvectors, which motivates the use of principal components combining (PCC) [4] to reduce receiver complexity. The PCC vector $\boldsymbol{f}_i$ is the SNR maximizing (BER minimizing) vector constrained to lie in the subspace spanned by the K_{pcc} principal eigenvectors of $\boldsymbol{R}_h(0)$: [4]

$$\boldsymbol{f}_i = \underbrace{\boldsymbol{U}_{K_{\text{pcc}}}}_{\tilde{\boldsymbol{U}}_{K_{\text{pcc}}}} \underbrace{\boldsymbol{\Theta}\,\boldsymbol{\Theta}^T \boldsymbol{U}_{K_{\text{pcc}}}^T \boldsymbol{h}_i}_{\tilde{\boldsymbol{z}}_i}, \tag{21}$$

where $\boldsymbol{U}_{K_{\text{pcc}}}$ collects the K_{pcc} principal eigenvectors of $\boldsymbol{R}_h(0)$, and $\boldsymbol{\Theta}$ is any $K_{\text{pcc}} \times K_{\text{pcc}}$ orthogonal matrix. The value K_{pcc} is a design choice that trades-off complexity and performance.

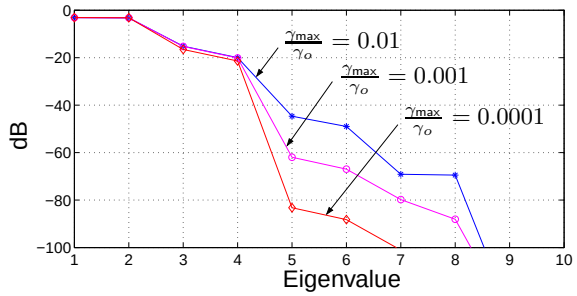

Fig. 3. Eigenvalues of channel autocorrelation matrix $\boldsymbol{R}_h(0)$ normalized to unit energy.

For operational convenience, the PCC vector can be applied in two stages: first, the scale-lag Rake received vector $\boldsymbol{r}_i$ is projected onto the principal eigenvector subspace: $\tilde{\boldsymbol{r}}_i = \tilde{\boldsymbol{U}}_{K_{\text{pcc}}}^T \boldsymbol{r}_i$; second, the projection is maximal ratio combined: $\hat{b}_i = \tilde{\boldsymbol{z}}_i^T \tilde{\boldsymbol{r}}_i$. The projection matrix $\tilde{\boldsymbol{U}}_{K_{\text{pcc}}}$ describes the channel statistics (scale spread, delay spread), which change slowly and thus can be easily learned by the receiver (e.g., [10]). The parameters $\tilde{\boldsymbol{z}}_i$ represent the channel realization, which changes quickly, and hence must be tracked using, e.g., decision-directed LMS or RLS. We will perform a study of adaptive solutions in future work.

In Fig. 4, we show the bit error rate (BER) performance of the PCC with perfect channel knowledge for increasing values of K_{pcc}—the number of principal components used in the receiver. The BER expression can be found in [9]. Recall from Fig. 3 that $\boldsymbol{R}_h(0)$ gives four non-negligible eigenvalues; hence, the scale-lag Rake exploits full channel diversity for $\bar{K} \geq 4$, as evidenced in Fig. 4.

5. CONCLUSION

In this paper, we studied the correlation structure of the fingers of the scale-lag Rake receiver and showed that the time-variability of the channel is captured in the *normalized scale spread* parameter $\frac{\gamma_{\max}}{\gamma_o}$. We also suggested incorporating PCC into the scale-lag Rake as a means of reducing complexity while maintaining performance. The analysis applies to radio-frequency UWB systems and wideband acoustic systems, where narrowband assumptions are invalid.

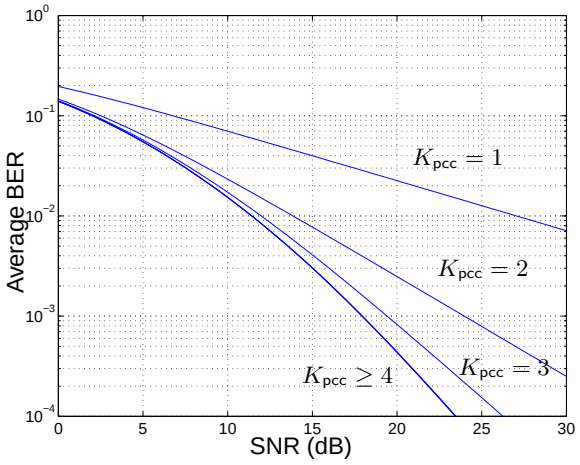

Fig. 4. BER performance of scale-lag Rake receiver using PCC with various values of $\bar{K}$. Normalized scale spread is $\frac{\gamma_{\max}}{\gamma_o} = 0.01$, and normalized delay spread is $\frac{\tau_{\max}}{T_o} = 1$.

A. AVERAGE AMBIGUITY FUNCTION PRODUCT APPROXIMATION

The approximation of (14) is based on the approximation of the expected ambiguity function product $\mathrm{E}[\chi(a,\tau)\chi(a',\tau')]$. The use of a random spreading code simplifies the computation

$$\mathrm{E}[\chi(a,\tau)\chi(a',\tau')] = \frac{1}{N_p^2} \sum_{i,j,k,l} \mathrm{E}[c_i c_j c_k c_l] \chi_p(a, \tau + (ai - j)T_o)\chi_p(a', \tau' + (a'k - l)T_o), \tag{22}$$

where $\chi_p(a,\tau) = \int p(t)\frac{1}{\sqrt{a}} p\left(\frac{t-\tau}{a}\right) dt$ is the ambiguity function of the pulse shape. The number of summation terms in (22) can be reduced by noting that

$$\mathrm{E}[c_i c_j c_k c_l] = \begin{cases} \mathrm{E}[c_i^4] & i = j = k = l, \\ \mathrm{E}[c_i^2]^2 & i = j,\ k = l,\ i \neq k, \\ \mathrm{E}[c_i^2]^2 & i = k,\ j = l,\ i \neq j, \\ \mathrm{E}[c_i^2]^2 & i = l,\ j = k,\ i \neq j, \\ 0 & \text{else.} \end{cases} \tag{23}$$

Hence, we need only compute the non-zero terms outlined in (23). We will find that only the second case will produce a non-negligible contribution. In the following, we make the change of variables $a = 1 + \frac{\bar{\gamma}}{N_p}$ to facilitate the approximation.

The absolute value of the sum of the terms in (22) for the case $i = j = k = l$ is upper bounded by

$$\sum_{i=0}^{N_p-1} \frac{\mathrm{E}[c_i^4]}{N_p^2} \left|\chi_p\left(1+\tfrac{\bar{\gamma}}{N_p}, \tau+\tfrac{\bar{\gamma} i T_o}{N_p}\right) \chi_p\left(1+\tfrac{\bar{\gamma}'}{N_p}, \tau'+\tfrac{\bar{\gamma}' i T_o}{N_p}\right)\right|$$

$$\approx \frac{\mathrm{E}[c_i^4]}{N_p} \int_0^1 \left|\chi_p(1, \tau + x\bar{\gamma}T_o)\chi_p(1, \tau' + x\bar{\gamma}'T_o)\right| dx \tag{24}$$

$$\leq \frac{\mathrm{E}[c_i^4]}{N_p} \tag{25}$$

The approximation in (24) is tight when a and a' are near unity and the number of chips N_p is large. The inequality in (25) follows from the pulse having bounded energy, i.e., $\chi_p(a,\tau) \leq 1, \forall\, a,\tau$. Hence, for a large number N_p of chips, the sum of the terms in the first case of (23) is negligible.

For the second case, $i=j,\ k=l,\ i\neq k$, we have

$$\begin{aligned}
&\sum_{i,k\neq i} \frac{\mathrm{E}[c_i^2]^2}{N_p^2}\chi_p\left(1+\tfrac{\bar\gamma}{N_p},\tau+\tfrac{\bar\gamma i T_o}{N_p}\right)\chi_p\left(1+\tfrac{\bar\gamma'}{N_p},\tau'+\tfrac{\bar\gamma' k T_o}{N_p}\right)\\
&\quad\approx \mathrm{E}[c_i^2]^2\int_0^1\chi_p(1,\tau+x\bar\gamma T_o)dx\int_0^1\chi_p(1,\tau'+x\bar\gamma' T_o)dx\\
&\quad\approx \mathrm{E}[\chi(a,\tau)]\,\mathrm{E}[\chi(a',\tau')] \qquad (26)
\end{aligned}$$

For the third case, $i=k,\ j=l,\ i\neq j$, we have

$$\begin{aligned}
&\sum_{i,j\neq i}\frac{\mathrm{E}[c_i^2]^2}{N_p^2}\Big|\chi_p\left(1+\tfrac{\bar\gamma}{N_p},\tau+(\tfrac{\bar\gamma i}{N_p}+i-j)T_o\right)\\
&\qquad\chi_p\left(1+\tfrac{\bar\gamma'}{N_p},\tau'+(\tfrac{\bar\gamma' i}{N_p}+i-j)T_o\right)\Big|\\
&\quad\approx\sum_{i,j}\frac{\mathrm{E}[c_i^2]^2}{N_p^2}\Big|\chi_p\left(1,\tau+(\tfrac{\bar\gamma i}{N_p}+i-j)T_o\right)\\
&\qquad\chi_p\left(1,\tau'+(\tfrac{\bar\gamma' i}{N_p}+i-j)T_o\right)\Big| \qquad (27)\\
&\quad\leq\sum_{i=0}^{N_p-1}\frac{2\,\mathrm{E}[c_i^2]^2}{N_p^2}\;=\;\frac{2\,\mathrm{E}[c_i^2]^2}{N_p} \qquad (28)
\end{aligned}$$

As before, the approximation in (27) is tight when a and a' are close to unity. Since the pulse is time-limited to T_o seconds, the function $\chi_p(1,x)$ is non-zero only when $|x|<T_o$. Therefore, given $\bar\gamma$ and τ, for each $i\in 1,2,\ldots,N_p-1$, there is at most two values of j such that $|\frac{\tau}{T_o}+\frac{\bar\gamma i}{N_p}+i-j|<1$. This observation, combined with the fact that $|\chi_p(a,\tau)|<1,\ \forall\, a,\tau$, leads to the inequality in (28). Thus, for a large number N_p of chips, the sum of the terms in the third case is negligible. Similarly, the sum of the terms in the fourth case $i=l,\ j=k,\ i\neq j$ can be shown to be negligible.

In summary, we have that the ambiguity function is approximately uncorrelated across scale and lag when the number of chips N_p is large,

$$\begin{aligned}
&\mathrm{E}[\chi(a,\tau)\chi(a',\tau')]\approx\mathrm{E}[\chi(a,\tau)]\,\mathrm{E}[\chi(a',\tau')],\\
&\quad\approx\mathrm{E}[c_i^2]^2\int_0^1\chi_p(1,\tau+x\bar\gamma T_o)dx\int_0^1\chi_p(1,\tau'+x\bar\gamma' T_o)dx,\\
&\quad=\bar\chi\left(\frac{a-1}{\gamma_o},\frac{\tau}{T_o}\right)\bar\chi\left(\frac{a'-1}{\gamma_o},\frac{\tau'}{T_o}\right). \qquad (29)
\end{aligned}$$

where $\bar\chi\,(\bar\gamma,\bar\tau)$ is defined in (16), and where $\bar\gamma := (a-1)N_p = (a-1)/\gamma_o$ and $\bar\gamma' := (a'-1)N_p = (a'-1)/\gamma_o$.

The approximation (29) is tight since we assume that a and a' are near unity and the number of chips N_p is large. Hence, after making the approximations[4] $\frac{a_o^m}{a}\approx 1+m\gamma_o-(a-1)$ and $\frac{nT_o a_o^m-\tau-i(a-1)T_s}{a}\approx nT_o-\tau-i(a-1)T_s$, we have that the correlation (14) can be approximated by (15)

[4]Note that $a_o^m\approx 1+m\gamma_o$, and $1/a\approx 1-(a-1)$.

B. AMBIGUITY FUNCTION FOR SECOND-DERIVATIVE GAUSSIAN CHIP PULSE

The closed-form ambiguity function expression for the unit energy 2^{nd}-derivative Gaussian pulse is quickly derived by using Parseval's theorem to perform the inner product calculation in the frequency domain:

$$\begin{aligned}
\chi_p(a,\tau) &= \int_{-\infty}^{\infty}\frac{1}{\sqrt{a}}p\left(\frac{t-\tau}{a}\right)p(t)dt, \qquad (30)\\
&= \int_{-\infty}^{\infty}\sqrt{a}\exp(-j2\pi\tau)P(af)P^*(f)df, \qquad (31)
\end{aligned}$$

where the Fourier transform $P(f)$ of the pulse $p(t)$ is

$$P(f) \;=\; \frac{\sqrt{f_o}\sqrt[4]{32\pi}}{\sqrt{3}}\frac{2}{\sqrt{\pi f_o^2}}\left(\frac{f}{f_o}\right)^2 e^{-\frac{f^2}{f_o^2}-j\pi f T_o}. \qquad (32)$$

We complete the square of the argument of the exponential in (31) and make use of the expression of the fourth Gaussian moment to write the solution as

$$\begin{aligned}
\chi_p(a,\tau) \;=\; f(a)\Big(&4\pi^4 g^4(a,\tau)-12\pi^2 g^2(a,\tau)(1+a^2)\\
&+3(1+a^2)^2\Big)\exp\left(-\frac{\pi^2 g^2(a,\tau)}{1+a^2}\right), \qquad (33)
\end{aligned}$$

where $f(a)=\frac{4}{3}\sqrt{\frac{2a^5}{(1+a^2)^9}}$ and $g(a,\tau)=f_o\tau+(a-1)f_oT_o/2$.

The expression for $\bar\chi(\bar\gamma,\bar\tau)=\mathrm{E}[c_i^2]\int_0^1\chi_p(1,(\bar\tau+x\bar\gamma)T_o)dx$, using the 2^{nd}-derivative Gaussian pulse follows from the closed-form expression of the pulse ambiguity function (33).

C. REFERENCES

[1] J. Proakis, *Digital Communications*. New York, NY: McGraw-Hill, 3rd ed., 1995.

[2] R. Balan, H. V. Poor, S. Rickard, and S. Verdú, "Time-frequency and time-scale canonical representations of doubly spread channels," *Proc. European Signal Processing Conf.*, Sep. 2004.

[3] A. R. Margetts, P. Schniter, and A. Swami, "Scale-lag diversity reception in mobile wideband channels," *Proc. IEEE Internat. Conf. on Acoustics, Speech, and Signal Processing*, Mar. 2005.

[4] M.-S. Alouini, A. Scaglione, and G. B. Giannakis, "PCC: Principal components combining for dense correlated multipah fading environments," *Proc. IEEE Vehicular Technology Conference*, vol. 5, pp. 2510–2517, Sept. 2000.

[5] M. Win and R. Scholtz, "Ultra-wide bandwidth time-hopping spread-spectrum impulse radio for wireless multiple-access communications," *IEEE Trans. on Communications*, vol. 48, pp. 679–689, Apr. 2000.

[6] B. M. Sadler and A. Swami, "On the performance of episodic UWB and direct-sequence communication systems," *IEEE Trans. on Wireless Communications*, 2004. accepted for publication.

[7] D. Swick, "Wideband ambiguity function of pseudo-random sequences: An open problem," *IEEE Trans. on Information Theory (correspondence)*, July 1968.

[8] A. M. Sayeed and B. Aazhang, "Joint multipath-doppler diversity in mobile wireless communications," *IEEE Trans. on Communications*, vol. 47, pp. 123–132, Jan. 1999.

[9] A. R. Margetts and P. Schniter, "Joint scale-lag diversity in mobile wideband communication systems," *Proc. Asilomar Conf. on Signals, Systems and Computers*, Nov. 2004.

[10] B. Yang, "Projection approximation subspace tracking," *IEEE Trans. on Signal Processing*, vol. 43, pp. 95–107, Jan. 1995.